

Bonding-site dependence of surface resistivity: CO on epitaxial Cu(100) films

Chang Liu and R. G. Tobin

Department of Physics and Astronomy, Tufts University, Medford, Massachusetts 02155

(Received 10 August 2006; accepted 17 January 2007; published online 23 March 2007)

The authors have measured the contribution of CO adsorbed on different bonding sites to the resistivity of epitaxial Cu(100) films. Through an analysis of the correlation between surface resistivity and temperature-programmed desorption measurements, CO on terraces is found to affect the resistance much more strongly than CO on defect sites. Two possible explanations are considered: a reduced scattering cross section of defect CO owing to the different local electronic structure at defect sites or strong scattering by the bare defect that is not significantly affected by the adsorption of CO. © 2007 American Institute of Physics. [DOI: 10.1063/1.2672832]

INTRODUCTION

Mechanisms of adsorbate-induced changes in surface resistivity have received a great deal of attention in recent years,¹ owing to the importance of this subject to such fields as tribology, thin films, sensing, and nanotechnology. Surface resistivity provides a straightforward and powerful probe of adsorption kinetics²⁻⁴ and interadsorbate interactions,⁵ and is central to the understanding of atomic-scale friction,⁶⁻⁹ electromigration,¹⁰ and adsorbate effects on the electrical resistance of metallic nanowires¹¹⁻¹³ and carbon nanotubes.^{14,15}

Our current understanding of surface resistivity is based on ideas first proposed by Fuchs¹⁶ and Sondheimer,¹⁷ and developed and expanded by Persson and Volokitin.^{7,18-22} For chemisorbed molecules on metals, the resistance change is attributed primarily to the diffuse scattering of conduction electrons, although some previous experimental results remain unexplained within that model.^{1,23-25} The locally perturbed electronic structure due to each adsorbate acts as a scattering center, disrupting the translational symmetry of the smooth surface and decreasing the electrical conductivity in a region extending from the surface to a depth on the order of the electron mean free path ℓ_B . The change in dc resistivity of the film can be written as¹

$$\frac{\Delta\rho}{\rho_B} = \frac{3}{16} \frac{\ell_B}{t} n_a \Sigma, \quad (1)$$

where ρ_B is the bulk resistivity, t is the thickness of the metal, n_a is the surface density of the adsorbates, and Σ is the scattering cross section per adsorbate. Because the resistivity change $\Delta\rho$ arises from the direct interaction of the conduction electrons with the adsorbate, it is a first layer effect. Subsequent layers grown on top of the first chemisorbed layer have negligible effect on the metal's conductivity.⁴

If there is a single adsorbate species and a single type of adsorption site, and there are no interactions between the adsorbates, the cross section Σ will be constant and the resistance will vary linearly with the coverage. Such a linear dependence has been observed for CO on Cu(100),^{3,26} for C₂H₂ on Cu(100),³ and for O on Cu(100).⁵

Interadsorbate interactions, either within a homogeneous layer or between different coadsorbed species, can cause the scattering cross section to change. There have been indications of such changes in a few systems such as S on Cu(100),^{5,27} coadsorption of CO with C₂H₄ on Cu(111),²⁸ and O on Cu(100) with preadsorbed S.²⁹ Interadsorbate interactions among S atoms⁵ or between O and S (Ref. 29) can reduce the scattering cross section of all the adsorbed atoms as the S coverage increases, while the interaction of CO with C₂H₄ results in a greater change in resistance than the sum of the individual changes for each species.²⁷

If the surface contains multiple possible bonding sites for the adsorbate, such as at steps and on terraces, it is possible for the scattering cross section Σ to be different at the various sites, even in the absence of interadsorbate interactions. This situation would lead to a generalization of Eq. (1):

$$\frac{\Delta\rho}{\rho_B} = \frac{3}{16} \frac{\ell_B}{t} \sum_i n_{a,i} \Sigma_i, \quad (2)$$

where the sum runs over the different types of bonding site. We are not aware of previous experiments that clearly show such an effect. Hu and Hirschmugl speculated that the highly nonlinear coverage dependence of the surface resistivity for S on Cu(100) was due to a high scattering cross section for S on defect sites and a near-zero cross section on terrace sites.²⁷ Subsequent experiments in our laboratory, however, showed that increasing the defect density had no influence on the shape of the resistance versus coverage curve,⁵ indicating that the nonlinearity was caused by interadsorbate interactions rather than site-to-site variations.

Our present experiments examine the surface resistivity due to CO on an epitaxial Cu(100) film with a high density of surface defects. A statistical analysis of the correlation of the adsorbate-induced resistivity with the CO coverages on the different bonding sites (as determined with temperature-programmed desorption) demonstrates that CO on terraces makes a much greater contribution to the surface resistivity, per adsorbed molecule, than CO on defects. Indeed the data are consistent with a zero or even slightly negative contribu-

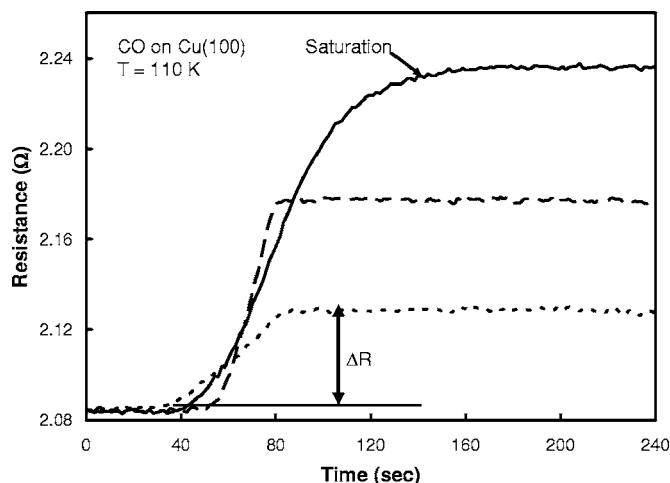


FIG. 1. Resistance change of 50 nm Cu(100) film during CO dosing at 110 K. During the CO exposure the resistance increases by an amount ΔR . The three curves correspond to three different CO exposures.

tion from CO on defects. We will discuss possible explanations for this striking difference between the sites.

EXPERIMENTAL PROCEDURES

The samples were epitaxial Cu(100) films, 50 nm thick, grown *in situ* in ultrahigh-vacuum (UHV, base pressure of 7×10^{-11} Torr) on 9×28 mm² Si(100) substrates. Contact strips (50 nm Ag on top of 10 nm Cr) were deposited *ex situ*. The sample was then etched for 60 s in a 10% aqueous HF solution to remove the native oxide and passivate the surface by terminating the dangling Si bonds with H atoms. After the sample was loaded into the UHV chamber via a high-vacuum load lock it was baked at 725 K for 15 min. Copper was deposited by thermal evaporation from a well-outgassed filament at a rate of ~ 0.1 nm/s with a sample temperature of 298 ± 2 K. Previous studies have demonstrated that these procedures result in epitaxial (100)-oriented films with root-mean-square surface roughness of 1–2 nm.³⁰ Details of sample preparation have been reported elsewhere.^{5,25,30}

An ac four-terminal technique was used to measure the film resistance, with a 1.0 mA rms current modulated at 3 kHz. The films' resistance was 3–4 Ω at $T=298$ K and 1–2 Ω at $T=110$ K, two to four times higher than that of pure bulk Cu of the same dimensions. This higher resistance is probably due in part to a high resistance buffer layer at the Si–Cu interface³⁰ and in part to the relatively high density of defects on the sample surface,^{5,30} as well as to possible impurities and defects in the bulk.

Following copper deposition, the sample was cooled to ~ 110 K and exposed to CO gas using a multihole effusive doser with an enhancement factor of 15–20.³¹ During CO exposure the electrical resistance of the Cu film was measured simultaneously. Figure 1 presents three examples of the resistance change as a function of time. The resistance rises during the CO exposure and then reaches a steady value when the CO dose is terminated. In the top curve, the CO exposure was continued until no further change in resistance was observed, indicating saturation of the surface with adsorbed CO.

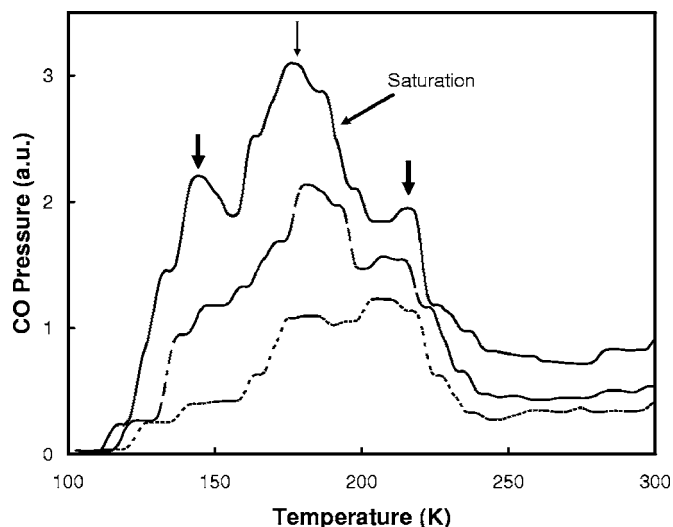


FIG. 2. Temperature-programmed desorption from three coverages of CO on 50 nm Cu(100) films exposed at 110 K. The three identifiable features are indicated with arrows.

Following each CO exposure, a temperature-programmed desorption (TPD) experiment was carried out with a ramp rate of 5 K/s. Figure 2 shows CO desorption traces for the three CO exposures from Fig. 1. The temperature ramp was stopped at 300 K to prevent reaction of the copper film with the silicon substrate, which occurs rapidly at temperatures above 450 K. The sample was then recooled to 110 K and the experiment was repeated with a different CO exposure. Typically four to five such experimental cycles would be carried out on a given sample; then a new substrate was prepared and a new Cu film deposited for the next experimental run. Because of the strong temperature dependence of the copper film's resistance, we could not detect the small resistance changes associated with CO desorption during the TPD experiments.

Three distinct features can be identified in the TPD traces, with peak desorption temperatures of approximately 135, 180, and 220 K. Similar features have been observed in studies of CO adsorption on vicinal Cu(100) surfaces.^{32,33} The 220 K feature, which is most prominent at the lowest coverages, was attributed to CO adsorbed on defect sites.^{32,33} On our samples this feature has a relatively high intensity, accounting for about 20% of the total desorbed CO at saturation, indicating a high defect concentration. The defect-site peak intensity is high compared to the single crystal used in Ref. 32 but comparable to that reported for low coverage CO on Cu(221) in Ref. 33. The feature at 180 K, which has the largest intensity at saturation, can be assigned to CO on flat (100) terraces.^{32,33} In separate measurements on a smooth (100) single crystal, only the 180 K feature was observed.³⁴

The identification of the ~ 135 K feature is problematic. A similar feature was observed in Refs. 32 and 33, but only at the highest coverages, and was attributed to compressed CO in regions with local coverage >0.5 ML,³² where CO–CO repulsion leads to a reduction in adsorption energy.³⁵ In our measurements, however, it is seen even at relatively low coverages (e.g., the middle curve of Fig. 2). A possible explanation is that the high defect concentration ob-

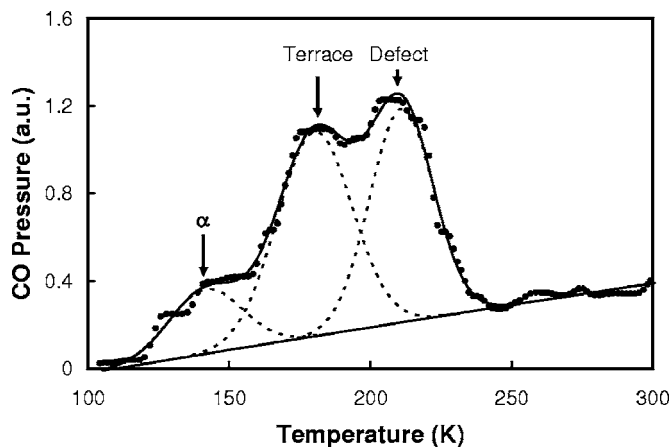


FIG. 3. Analysis of TPD data (points) as the sum of three Gaussian functions plus a quadratic base line. The integrated area of each Gaussian is taken as a measure of the coverage of the corresponding CO species.

structs CO diffusion, leading to regions of locally high CO coverage even when the average CO coverage is relatively low. In this paper we simply designate this feature as the α peak, without further assumptions as to its origins. Our primary focus will be on the terrace and defect peaks, which together account for about 80% of the overlayer at saturation.

In order to determine the relative populations of the three CO species, each TPD curve was decomposed into a sum of three Gaussians on top of a quadratic base line, as illustrated in Fig. 3. The integrated area under each Gaussian is then taken as a measure of the population of the corresponding CO species. As a consistency check, the sum of the integrated areas of the three Gaussians always agreed within 5% with the integrated area under the experimental TPD curve (after base line subtraction). The fitted peak temperatures were also stable and reproducible, with standard deviations of about 6 K.

Figure 4 shows the variation of the individual peak intensities with the total integrated TPD signal (that is, with total CO coverage). At all coverages shown, the terrace peak has the highest integrated intensity. At low coverages, the defect peak is comparable in strength to the terrace peak, indicating preferential occupation of defect sites, as expected from their higher binding energy.³³ As the total coverage increases, however, the defect-site intensity increases less rapidly than the terrace-site intensity, so that at saturation coverage the defects account for only about 20% of the total CO population. Compared to a single crystal surface this is still a very high fraction, indicative of the relative roughness of the epitaxial film on the atomic scale. Similar behavior, though with a lower defect-site fraction, was observed by Borguet and Dai on a vicinal Cu(100) crystal.³² At all coverages the α peak is the weakest, representing at most about 20% of the total.

The integrated intensity of an individual TPD peak is a measure of the initial population of the corresponding CO species only if there is no net migration from one site to another as the sample is heated during the TPD experiment. In the event that migration occurs from the bonding sites of low activation energy to those of high activation energy, the

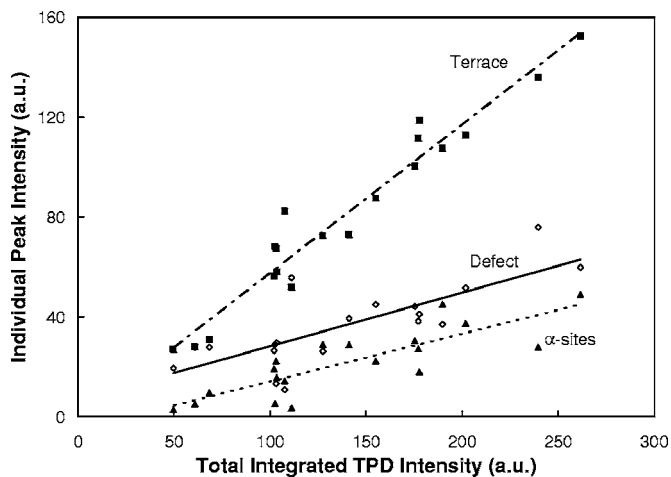


FIG. 4. Variation of the individual TPD peak intensities with the total integrated TPD intensity (i.e., CO coverage). The lines are linear fits.

population of the latter sites will be overestimated. We have carried out experiments with CO isotopes that show that exchange of CO between binding sites does occur in the relevant temperature range, so it is likely that site-to-site migration has some effect on our quantitative results. As we will discuss below, however, our primary conclusion—that the different CO species make very different contributions to the surface resistivity, and in particular that the terrace CO contributes far more strongly than CO on defect sites—is not significantly affected.

RESULTS AND ANALYSIS

In order to determine the relative contributions of the various CO species to the film's resistance, we examine the correlation of the adsorbate-induced resistance change ΔR with the TPD intensities corresponding to the individual species, I_α , I_t , and I_d . We consider a general linear model³⁶ with separate resistance contributions for the various sites:

$$\Delta R = \sum_{\text{sites}} a_i I_i = a_\alpha I_\alpha + a_t I_t + a_d I_d. \quad (3)$$

We have carried out a multiple linear regression analysis³⁷ on all our data (a total of 18 separate CO exposures on four separate, but identically prepared samples) to find the values of the coefficients a_α , a_t , and a_d that best fit the experimental results and to evaluate the statistical significance of each site's contribution.

Table I presents the best-fit results for the general linear model described by Eq. (3), as well as for constrained models in which one or more of the coefficients is set to zero, omitting the corresponding site(s) from the analysis, and for a model in which all sites make equal contributions ($a_\alpha = a_t = a_d$). The quantity p represents the probability that the difference in quality of fit between the constrained and unconstrained models could result from random variation, rather than from a meaningful difference between the models. A low value of p (typically <0.05) indicates that the corresponding constrained model is excluded by the data; in the table the excluded constraints are listed in parentheses. Thus the second row of the table shows that the experimental data

TABLE I. Fitting parameters and statistical significance for linear regression analysis of the correlation between resistance change ΔR and the individual TPD peak intensities I_α , I_t , and I_d , as described by Eq. (3). The first row represents a fit in which all three CO species are included. In the other lines one or more term constraints are applied to the model. Parentheses indicate constraints that are excluded by the data at a 99% confidence level.

Constraint	$a_\alpha (\times 10^{-4})$	$a_t (\times 10^{-4})$	$a_d (\times 10^{-4})$	p
None	6.0 ± 5.2	13.2 ± 2.2	-3.8 ± 3.1	...
$(a_\alpha = a_d = a_t)$	7.6 ± 0.4	7.6 ± 0.4	7.6 ± 0.4	0.008
$(a_t = 0)$	29.7 ± 6.2	0	10.5 ± 3.8	2×10^{-5}
$a_\alpha = a_d = 0$	0	13.1 ± 0.5	0	0.22
$a_\alpha = 0$	0	15.0 ± 1.5	-4.5 ± 3.1	0.27
$a_d = 0$	7.1 ± 5.2	11.2 ± 1.5	0	0.24

exclude a model in which all three CO species contribute equally to the resistance. The third row indicates, not surprisingly, that a model in which terrace CO makes no contribution is also excluded.

On the other hand, high values of p (typically >0.1) indicate that there is no statistically meaningful difference between the constrained and unconstrained models. Thus the last three rows of the table show that it makes little difference to the quality of fit if the α or defect-bonded CO or both is assumed to make zero contribution to the resistance. Even though the unconstrained fit gives nonzero values for the coefficients a_α and a_d , the data are also consistent with zero values for those coefficients.

The central conclusion to be drawn from the analysis summarized in Table I is that the resistance change is dominated, even on a per-molecule basis, by CO bonded on terrace sites. Figure 5 further emphasizes this point. It shows the correlation of the measured resistance change with the resistance change predicted by three models: by the general model with all sites included [Fig. 5(a) and the top row of Table I] and by two constrained models, one in which *only* terrace CO is considered [$a_\alpha = a_d = 0$, Fig. 5(b) and fourth row of Table I] and one in which all sites are assumed to make equal contributions [Fig. 5(c) and second row of Table I]. For Fig. 5(b) the abscissa is directly proportional to I_t and for Fig. 5(c) to $I_{\text{total}} = I_\alpha + I_t + I_d$. The shaded area indicates the mean-square deviation of the experimental data from the model; its size is thus a rough indicator of the quality of the fit.

Since terrace CO accounts for virtually all of the surface resistivity and constitutes the largest component of the total TPD intensity, all three models account reasonably well for the data, and the differences in quality of fit are rather subtle. Nevertheless close inspection of Fig. 5 reveals that there is little difference in quality of fit between Figs. 5(a) and 5(b), but Fig. 5(c) has a noticeably higher mean-square deviation. That is, a model in which *only* terrace CO contributes to the surface resistivity does a better job of explaining the data than one in which all sites contribute equally, and does almost as well as a completely general model in which all three sites contribute.

Finally, it is worth noting that, when the terrace sites are included in the fit, the defect-site coefficient a_d comes out

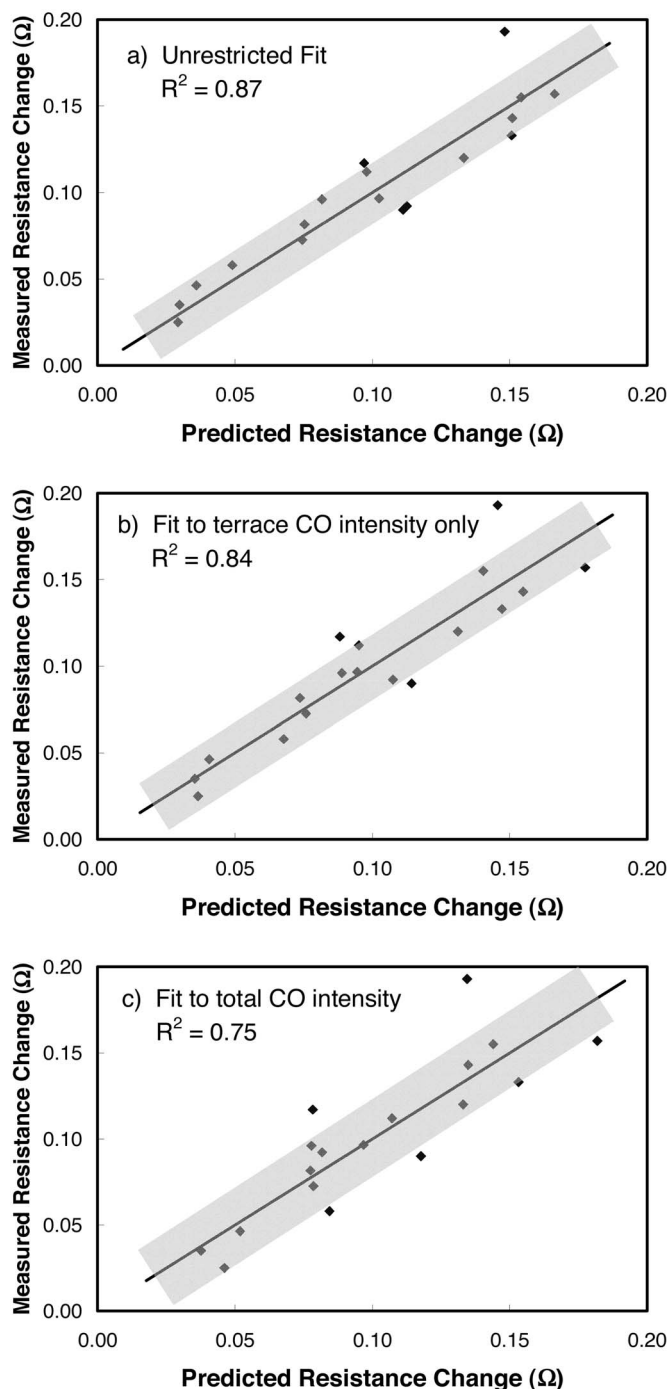


FIG. 5. Comparison of three models for the dependence of the resistance change on TPD intensity. The line represents an ideal fit, and the shaded areas indicate the mean-square deviation between the data and the model. (a) Unrestricted linear fit, with independent coefficients a_α , a_t , and a_d . (b) Fit to intensity of the terrace peak only: $a_\alpha = a_d = 0$. The difference between this fit and the unrestricted fit is not statistically significant ($p=0.22$). (c) Fit to the total TPD intensity: $a_\alpha = a_t = a_d$. This fit is significantly worse than the other two ($p=0.008$).

negative, suggesting that adsorption of CO on defect sites tends to *decrease* the resistance of the film. In view of the large uncertainty and marginal statistical significance of a_d , this point should not be overemphasized, but a possible explanation will be discussed in the next section.

As we discussed in the last section, it is possible that some movement of CO from lower to higher binding energy

sites takes place during the TPD measurement. We use a simple model to analyze the possible effects of CO migration on our results. We assume that at all coverages a constant fraction γ of terrace CO migrates to defect sites and desorbs in the 220 K peak, while a constant fraction β of α -site CO migrates to terrace sites and desorbs in the 180 K peak. Migration from α sites to defects is neglected. This model gives a linear relationship between measured TPD intensities and actual site coverages θ ,

$$\begin{aligned} I_\alpha &\propto (1 - \beta)\theta_\alpha, \\ I_t &\propto \beta\theta_\alpha + (1 - \gamma)\theta_t, \\ I_d &\propto \gamma\theta_t + \theta_d. \end{aligned} \quad (4)$$

As a result, the true correlation coefficients a_i^r are linearly related to the measured coefficients a_i :

$$\begin{aligned} a_\alpha^r &= a_\alpha + (a_t - a_\alpha)\beta, \\ a_t^r &= a_t - (a_t - a_d)\gamma, \\ a_d^r &= a_d. \end{aligned} \quad (5)$$

Each coefficient is affected by migration *out* of the corresponding site but not by migration *in*. Thus the defect-site coefficient a_d^r is unaffected while the terrace-site coefficient is reduced.

We can set an upper limit on the fraction γ of terrace CO that desorbs in the defect-site peak by making the extreme and unrealistic assumption that *all* of the defect-site intensity originates from terrace CO; then $\gamma \leq I_d / (I_t + I_d)$. Based on our data, if γ is independent of coverage as assumed, then $\gamma \leq 0.12$. Using the measured values of a_t and a_d from Table I and taking their uncertainties into account, we find that a_t^r falls between 12.5 ($\gamma=0$) and 11.2 ($\gamma=0.12$ and assuming the maximum value of a_d). At worst, then, terrace-to-defect migration reduces the terrace-site coefficient by about 10% and does not change the defect-site coefficient. Thus our primary conclusion—that CO on terraces affects the surface resistivity much more than CO on defect sites—is not significantly affected.

Because the terrace-CO desorption peak is much larger than the α peak, we cannot use a similar method to set a meaningful limit on α -to-terrace migration (β). As a result, we cannot rule out the possibility that our analysis significantly underestimates the resistivity contribution of α -CO. If β is close to 1, it is even possible that $a_\alpha^r \approx a_t^r$. Our conclusions regarding the relative resistivity contributions of terrace and defect CO, however, would not be significantly changed.

DISCUSSION

The experimental results presented above clearly demonstrate that CO on different bonding sites makes markedly different contributions to the surface resistivity, with CO on the flat terraces having a much greater effect than CO adsorbed at defect sites; in fact the data are consistent with a *zero* contribution from defects.

Comparing Eq. (2) with Eq. (3) and assuming that the intensity I_i of a particular desorption peak is proportional to $n_{a,i}$, the surface concentration of CO on the corresponding site, the coefficients a_i from the multiple linear fit are proportional to the scattering cross sections Σ_i of the corresponding CO species. Within the scattering model of surface resistivity, then, our results suggest that CO at defect sites scatters conduction electrons much less effectively than CO at terrace sites. (An alternative interpretation will, however, be discussed below.) At first sight, this result appears counterintuitive. CO is more strongly bound at defect than at terrace sites, indicating a stronger adsorbate-metal interaction, which might be expected to result in stronger, rather than weaker, scattering. Moreover, the difference in binding energies is relatively small, on the order of 15%,³³ so it is surprising to find such a large difference in scattering cross section.

Persson's model of surface resistivity is based on the familiar Newns-Anderson model of adsorption, which has provided a fruitful framework for understanding a wide range of surface phenomena.^{19,38–40} In this model, hybridization between the adsorbate's molecular orbitals and the electronic states of the substrate gives rise to a broad adsorbate-derived electronic state that overlaps the Fermi level and is therefore partially occupied. Dynamic variations in the orbital's occupation couple the adsorbate's degrees of freedom—electronic, vibrational, and translational—to the metal's electronic states and facilitate the transfer of energy and momentum between the two. In Persson's analysis,¹⁹ the scattering cross section is determined largely by the width of the orbital in energy, Γ , and the adsorbate-derived density of states at the Fermi level, $\rho_a(E_F)$:

$$\Sigma = \frac{16k_F}{3n_B} \langle \sin^2 \theta \rangle_a \Gamma \rho_a(E_F). \quad (6)$$

Here k_F is the Fermi wave vector, n_B is the bulk electron density, and $\langle \sin^2 \theta \rangle_a$ is an average over scattering angles. For a given adsorbate and substrate material, variations in the surface resistivity per molecule (i.e., variations in Σ) are then associated with variations in the width or position in energy of the relevant orbital. Such an analysis was successfully used, for example, to explain the effects of CO–C₂H₄ interactions on surface resistivity.²⁸

The electronic structure and bonding of CO on Cu(100) have been intensively studied.^{41–43} In the standard picture, the CO $2\pi^*$ orbital hybridizes strongly with the narrow Cu d band and splits into bonding and antibonding components below and above the Fermi level, respectively.⁴² The low-energy tail of the antibonding orbital is believed to overlap the Fermi level and is assumed to dominate the electron dynamics.^{38,39,43} This general picture seems to be well supported by both experiment and theory, although there is also evidence of a weak π -derived state just below the Fermi level that could also make a contribution,⁴² and one theoretical study found a large role for the fully occupied 5σ state.⁴⁴

Nørskov, Hammer and co-workers have shown that bonding to transition metals is dominated by the position and width of the d band.^{40,43,45,46} At defect sites (e.g., steps), the metal atoms have lower coordination to neighboring surface-

metal atoms than terrace atoms, resulting in a local d band that is narrower and higher in energy.⁴⁰ Hybridization of the d band with the CO $2\pi^*$ orbital will cause the antibonding component to lie higher in energy than at terrace sites, and it can then be expected to have a lower density of states $\rho_d(E_F)$ and thus a lower scattering cross section Σ . (This is the reverse of the effect of coadsorbed C_2H_4 , in which hybridization of the CO $2\pi^*$ orbital with a higher-lying C_2H_4 orbital pushes the CO orbital closer to the Fermi level, increasing Σ .²⁸) This analysis provides at least a qualitative explanation for a reduced scattering cross section at defect sites.

Differences in electronic screening could also contribute to reduced scattering from CO at defect sites. Friedel oscillations in the local density of states can extend for several lattice spacings around an impurity⁴⁷ and can have significant effects on adsorbate-adsorbate interactions.^{48,49} This extended perturbation may contribute to the electron scattering cross section of the adsorbate and could be quite different for adsorbates on step and terrace sites. Scanning tunneling microscope images seem to show a less extensive perturbation for point defects near step edges than for those on terraces.⁴⁷

There is, however, another possibility, involving the scattering cross section of the bare defect, as well as that of the adsorbate. The surface resistivity model we have been considering implicitly assumes that the clean surface makes no contribution, so that the measured resistivity coefficient a_i is simply proportional to the scattering cross section Σ_i of CO on the corresponding site. This assumption is reasonable for terrace sites, since a smooth surface does not scatter electrons and so does not contribute to the resistivity.^{16,17} Defects, however, break the surface's translational symmetry, and can therefore act as scattering centers, even in the absence of adsorbates. Experiments in our laboratory showed that sputtering increases the surface resistivity of one of our Cu films by an amount comparable to an adsorbed monolayer,⁵ suggesting that the scattering cross section of a bare defect, Σ_d^b , is comparable to that of an adsorbed molecule.

If the bare defect is a significant scatterer, the measured coefficient a_d is a measure of the *difference* in cross section between the defect with and without adsorbed CO: $a_d \propto (\Sigma_d^{CO} - \Sigma_d^b)$, not simply of the cross section of the adsorbate. If the defect is already a strong scatterer, the *differential* effect of adding CO to the site could be small, even if the inherent scattering cross section of the adsorbate is significant. It is even possible for the differential effect to be negative, if the adsorbed CO reduces the scattering by the bare defect. This mechanism could explain the negative best-fit value of a_d in Table I (which is, however, of marginal statistical significance). A similar negative coefficient has been observed in hydrogen adsorption on Fe films with preadsorbed oxygen.⁵⁰

Further experimental and theoretical work will be needed to determine whether the small (and possibly negative) apparent contribution of defect-bonded CO to the surface resistivity arises from an inherently low scattering cross section, due to electronic structure effects, or from a large scattering cross section of the bare defect that is not significantly changed by the adsorption of CO.

CONCLUSION

Adsorbates bonded to defect sites generally have different properties from those bonded to flat terraces. Some properties, such as binding energy and vibrational frequencies, typically differ only modestly. Others, such as dissociation probability or chemical reactivity, can exhibit radical differences. The experiments here show that, for CO on Cu(100), the surface resistivity is in the latter category: Although the binding energy of CO at defects is only $\sim 15\%$ greater than at terrace sites,³³ the effect on surface resistivity for terrace CO is more than a factor of 2 greater than for CO on a defect site. Indeed the data are consistent with a zero contribution for CO on defects, and there is even a suggestion that the defect CO contribution is negative. These results may have important implications in applications such as chemical sensing in which the concentration of surface defects is high.

A reduced (but not negative) surface resistivity contribution for defect-bonded CO can be qualitatively explained using the Newns-Anderson model, taking into account the higher local d -band energy at defect sites.⁴⁰ It is also possible, however, that the apparently small, or even negative effect of defect-bonded CO is due to a large scattering cross section for the bare defect that is only modestly changed, and perhaps even reduced, by the adsorption of CO. Further investigation will be needed to distinguish between the two effects.

ACKNOWLEDGMENTS

The authors thank Russell Sargent for his help with the experiments. This work was supported in part by the Tufts Faculty Research Fund.

- ¹R. G. Tobin, Surf. Sci. **502–503**, 374 (2002).
- ²J. Dvorak, E. Borguet, and H.-L. Dai, Surf. Sci. **369**, L122 (1996).
- ³J. Dvorak and H.-L. Dai, J. Chem. Phys. **112**, 923 (2000).
- ⁴C.-L. Hsu, E. F. McCullen, and R. G. Tobin, Surf. Sci. **542**, 120 (2003).
- ⁵R. G. Tobin, Surf. Sci. **524**, 183 (2003).
- ⁶A. Dayo, W. Alnasrallah, and J. Krim, Phys. Rev. Lett. **80**, 1690 (1998).
- ⁷B. N. J. Persson, J. Chem. Phys. **98**, 1659 (1993).
- ⁸J. B. Sokoloff, Phys. Rev. B **52**, 5318 (1995).
- ⁹A. I. Volokitin and B. N. J. Persson, Phys. Rev. Lett. **94**, 086104 (2005).
- ¹⁰M. F. G. Hedouin and P. J. Rous, Phys. Rev. B **62**, 8473 (2000).
- ¹¹C. Z. Li, H. Sha, and N. J. Tao, Phys. Rev. B **58**, 6775 (1998).
- ¹²Z. Liu and P. C. Searson, J. Phys. Chem. B **110**, 4318 (2006).
- ¹³X. Qi and F. E. Osterloh, J. Am. Chem. Soc. **127**, 7666 (2005).
- ¹⁴G. U. Sumanasekera, C. K. W. Adu, S. Fang, and P. C. Eklund, Phys. Rev. Lett. **85**, 1096 (2000).
- ¹⁵V. M. Bermudez, J. Phys. Chem. B **109**, 9970 (2005).
- ¹⁶K. Fuchs, Proc. Cambridge Philos. Soc. **34**, 100 (1938).
- ¹⁷E. H. Sondheimer, Adv. Phys. **1**, 1 (1952).
- ¹⁸B. N. J. Persson, Surf. Sci. **269/270**, 103 (1992).
- ¹⁹B. N. J. Persson, Phys. Rev. B **44**, 3277 (1991).
- ²⁰B. N. J. Persson, Chem. Phys. Lett. **197**, 7 (1992).
- ²¹B. N. J. Persson and A. I. Volokitin, Surf. Sci. **310**, 314 (1994).
- ²²A. I. Volokitin and B. N. J. Persson, Phys. Rev. B **52**, 2899 (1995).
- ²³C.-L. Hsu, E. F. McCullen, and R. G. Tobin, Chem. Phys. Lett. **316**, 336 (2000).
- ²⁴E. F. McCullen, C.-L. Hsu, and R. G. Tobin, Surf. Sci. **481**, 198 (2001).
- ²⁵E. T. Krastev, D. E. Kuhl, and R. G. Tobin, Surf. Sci. **387**, L1051 (1997).
- ²⁶C. J. Hirschmugl, Y. J. Chabal, F. M. Hoffmann, and G. P. Williams, J. Vac. Sci. Technol. A **12**, 2229 (1994).
- ²⁷X. F. Hu and C. J. Hirschmugl, Surf. Sci. **490**, 69 (2001).
- ²⁸M. Hein, P. Dumas, A. Otto, and G. P. Williams, Surf. Sci. **465**, 249 (2000).
- ²⁹C. Liu and R. G. Tobin (unpublished).

- ³⁰E. T. Krastev, L. D. Voice, and R. G. Tobin, *J. Appl. Phys.* **79**, 6865 (1996).
- ³¹D. E. Kuhl and R. G. Tobin, *Rev. Sci. Instrum.* **66**, 3016 (1995).
- ³²E. Borguet and H.-L. Dai, *J. Chem. Phys.* **101**, 9080 (1994).
- ³³S. Vollmer, G. Witte, and C. Wöll, *Catal. Lett.* **77**, 97 (2001).
- ³⁴W. Lu and R. G. Tobin (unpublished).
- ³⁵J. C. Tracy, *J. Chem. Phys.* **56**, 2748 (1972).
- ³⁶We also tested models with a nonzero constant term and found no evidence for a statistically significant nonzero value. All of the analysis presented here therefore assumes a zero constant, as expressed in Eq. (3).
- ³⁷G. O. Wesolowsky, *Multiple Regression and Analysis of Variance* (Wiley, New York, 1976).
- ³⁸B. N. J. Persson and M. Persson, *Solid State Commun.* **36**, 175 (1980).
- ³⁹M. Hein, P. Dumas, M. Sinther, A. Priebe, P. Lilie, A. Bruckbauer, A. Pucci, and A. Otto, *Surf. Sci.* **600**, 1017 (2006).
- ⁴⁰B. Hammer, *Top. Catal.* **37**, 3 (2006).
- ⁴¹G. Blyholder, *J. Phys. Chem.* **68**, 2772 (1964).
- ⁴²A. Föhlisch, M. Nyberg, P. Bennich, L. Triguero, J. Hasselström, O. Karis, L. G. M. Pettersson, and A. Nilsson, *J. Chem. Phys.* **112**, 1946 (2000).
- ⁴³B. Hammer, Y. Morikawa, and J. K. Nørskov, *Phys. Rev. Lett.* **76**, 2141 (1995).
- ⁴⁴G. Volpilhac, M. F. Baba, and F. Achard, *J. Chem. Phys.* **97**, 2126 (1992).
- ⁴⁵B. Hammer and J. K. Nørskov, *Nature (London)* **376**, 238 (1995).
- ⁴⁶A. Nilsson, L. G. M. Petersson, B. Hammer, T. Bligaard, C. H. Christensen, and J. K. Nørskov, *Catal. Lett.* **100**, 111 (2005).
- ⁴⁷M. F. Crommie, C. P. Lutz, and D. M. Eigler, *Nature (London)* **363**, 524 (1993).
- ⁴⁸E. Borguet and H.-L. Dai, *J. Phys. Chem. B* **109**, 8509 (2005).
- ⁴⁹X. F. Hu and C. J. Hirschmugl, *Phys. Rev. B* **72**, 205439 (2005).
- ⁵⁰M. R. Shanabarger, *J. Vac. Sci. Technol. A* **4**, 623 (1986).